nature synthesis

Article

https://doi.org/10.1038/s44160-024-00595-5

Synthesis of azahexabenzocoronenium salts through a formal [3 + 3] cycloaddition strategy

Received: 16 September 2023

Accepted: 4 June 2024

Published online: 10 July 2024

Check for updates

Xinjiang Zhang[1], Donglin Li[2], Cheryl Cai Hui Tan[1], Fiona Hanindita[1], Yosuke Hamamoto[1], Adam S. Foster[3,4] ✉, Shigeki Kawai[2,5] ✉ & Shingo Ito[1] ✉

Heteroatom-embedded hexa-*peri*-hexabenzocoronene (HBC) molecules exhibit interesting properties depending on the number and position of the introduced heteroatoms and are promising materials for applications in organic electronics and supramolecular chemistry. However, their synthesis is quite limited because of the difficulty in selectively introducing heteroatoms into the HBC core, which poses a challenge in organic synthesis. Here we report a strategy for the in-solution synthesis of 3a^2-azahexa-*peri*-hexabenzocoronenium salts, which are cationic nitrogen-embedded HBC derivatives. The synthesis was enabled by the formal [3 + 3] cycloaddition of polycyclic aromatic azomethine ylides with cyclopropenes, as a three-atom dipolarophile, followed by mechanochemical intramolecular cyclization. Furthermore, on-surface polymerization of aza-HBC precursors was performed to synthesize aza-HBC-based chevron-like graphene nanoribbons. This study provides the possibility for the further use of nitrogen-embedded HBC derivatives in a variety of potential applications.

Hexa-*peri*-hexabenzocoronene (HBC; Fig. 1) is a discotic polycyclic aromatic molecule composed of 42 carbon atoms and 18 hydrogen atoms. Since its first synthesis in 1958 (refs. 1,2), HBC and its derivatives have emerged as the most prominent representatives of polycyclic aromatic molecules because of their extended π-conjugated surface, characterized by regularly aligned benzenoid hexagons[3–5]. The fascinating symmetrical structure and intriguing properties of HBC have fuelled extensive research on its synthesis and applications in supramolecular chemistry[6,7], organic electronics[3–5,8,9] and biology[10,11].

Given the profound importance of HBC molecules, the exploration of heteroatom-embedded HBC molecules presents a compelling avenue for research across a wide range of scientific disciplines[12–14]. The first synthesis of a nitrogen-containing HBC molecule was reported in 2002, when Draper successfully developed pyrimidine-fused HBCs (**A**) and their application as ligands in organometallic chemistry[15–17]. Later, Draper[18] and Jux[19] independently introduced a class of HBCs fused with a peripheral pyridine ring (**B**), which were subsequently converted to cationic analogues such as alkylpyridinium and pyridine oxide. While these HBC molecules feature nitrogen atoms at their periphery, the incorporation of heteroatoms into the internal framework remains an intricate and formidable challenge. The synthesis of HBC molecules with internal heteroatoms has been achieved mainly by on-surface synthesis, as exemplified by borazine-embedded HBC (**C**) in 2015 (ref. 20), pyrazine-embedded HBC (**D**) in 2017 (ref. 21) and pyridinium-embedded HBC (**E**) in 2021 (ref. 22), although the in-solution synthesis of **C** was later reported by the group of

[1]School of Chemistry, Chemical Engineering and Biotechnology, Nanyang Technological University, Singapore, Singapore. [2]Center for Basic Research on Materials, National Institute for Materials Science, Tsukuba, Japan. [3]Department of Applied Physics, Aalto University, Espoo, Finland. [4]Nano Life Science Institute (WPI-NanoLSI), Kanazawa University, Kanazawa, Japan. [5]Graduate School of Pure and Applied Sciences, University of Tsukuba, Tsukuba, Japan. ✉e-mail: adam.foster@aalto.fi; kawai.shigeki@nims.go.jp; sgito@ntu.edu.sg

https://doi.org/10.1038/s44160-024-00595-5

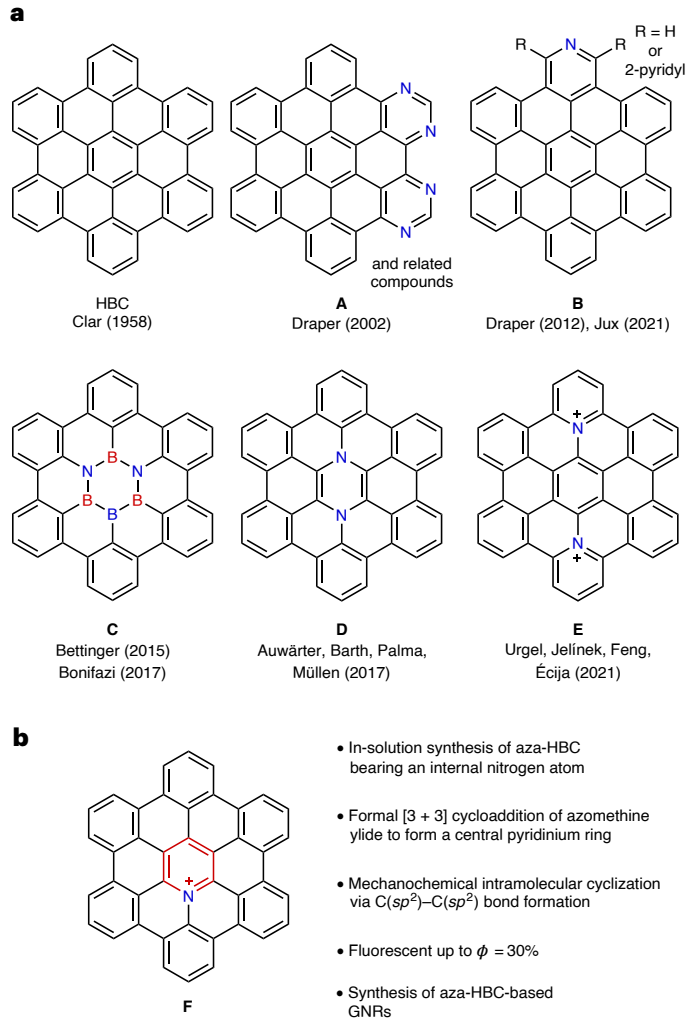

Fig. 1 | HBC derivatives. a, HBC and heteroatom-embedded HBC molecules **A**[15], **B**[18,19], **C**[20,23], **D**[21] and **E**[22] in the literature. **b**, Azahexabenzocoronenium **F** in this work.

Bonifazi[23,24]. It is important to note that on-surface synthesis, while feasible, inherently restricts the comprehensive investigation of their properties and hampers their practical application. Consequently, there is a pressing need for in-solution organic synthesis of heteroatom-embedded HBC molecules. Herein we report the in-solution synthesis of cationic nitrogen-embedded hexabenzocoronene derivatives **F**, namely, 3a^2-azahexa-*peri*-hexabenzocoroneniu m. The synthesis was achieved through a formal [3 + 3] cycloaddition of polycyclic aromatic azomethine ylides and cyclopropenes, which act as 'three-atomic dipolarophiles', followed by mechanochemical intramolecular cyclization, facilitating the formation of C(sp^2)–C(sp^2) bonds. The structure and properties of azahexabenzocoronenium **F** were investigated by various spectroscopic methods, which have been difficult to perform with other heteroatom-embedded HBC molecules bearing internal heteroatoms.

Figure 2 illustrates our synthetic design for cationic HBC molecule **F**, which is based on the 1,3-dipolar cycloaddition of polycyclic aromatic azomethine ylides **1** (refs. 25–32). It was previously reported that HBC molecule **D** was synthesized through [3 + 3] homodimerization of azomethine ylides **1** followed by oxidative cyclization on the metal surface (Fig. 2a)[21]. In our initial approach, therefore, we planned to adopt the same 1,3-dipolar cycloaddition strategy to synthesize azahexabenzocoronenium **F**. To construct its core structure, we need to perform [3 + 3] cycloaddition of azomethine ylide **1** with a three-atomic CCC unit (Fig. 2b), but this type of [3 + 3] cycloaddition reaction has never been reported. Consequently, we decided to develop a formal [3 + 3] cycloaddition using cyclopropene derivative **2** as a coupling partner. Since **2** is an alkene molecule, it can undergo 1,3-dipolar cycloaddition with polycyclic aromatic azomethine ylides **1** to yield the corresponding cycloadduct. The resulting azabicyclo[3.1.0]hexane system is expected to undergo skeletal rearrangement upon oxidation, forming the corresponding pyridinium ring[33,34]. Overall, this transformation can be considered a formal [3 + 3] cycloaddition of azomethine ylide **1** and cyclopropene **2**, with the latter serving as a three-atomic dipolarophile, ultimately leading to the formation of azahexabenzocoronenium **F**.

Results and discussion

Synthesis of π-extended pyridinium salts by formal [3 + 3] 1,3-dipolar cycloaddition

To validate our hypothesis, 1,3-dipolar cycloaddition of a polycyclic aromatic azomethine ylide derived from iminium salt **1a** and cyclopropene derivative **2a** (ref. 35) was performed in dimethyl sulfoxide at 120 °C, which yielded cycloadduct **3a** in nearly quantitative yield as a mixture of diastereomers with a ratio of 70:28 (Fig. 3a). The high reactivity of **2a** as an alkene leading to the high yield of **3a** is attributed to its inherent molecular strain in the cyclopropene structure[30]. The diastereomers of **3a** can be separated and isolated by silica gel column chromatography and further characterized by NMR spectroscopic analyses, mass spectrometric analyses and single-crystal X-ray diffraction analysis (Supplementary Fig. 65). Subsequently, **3a** was treated with 3.0 equivalents of chloranil, which serves as an oxidant, at 40 °C. This treatment induced a skeletal rearrangement, converting azabicyclo[3.1.0]hexane into the corresponding pyridinium ring. Notably, both isomers of **3a** underwent this transformation with high efficiency, providing π-extended pyridinium **4a** in high yields. This reaction was found to be versatile because it was successfully applied to

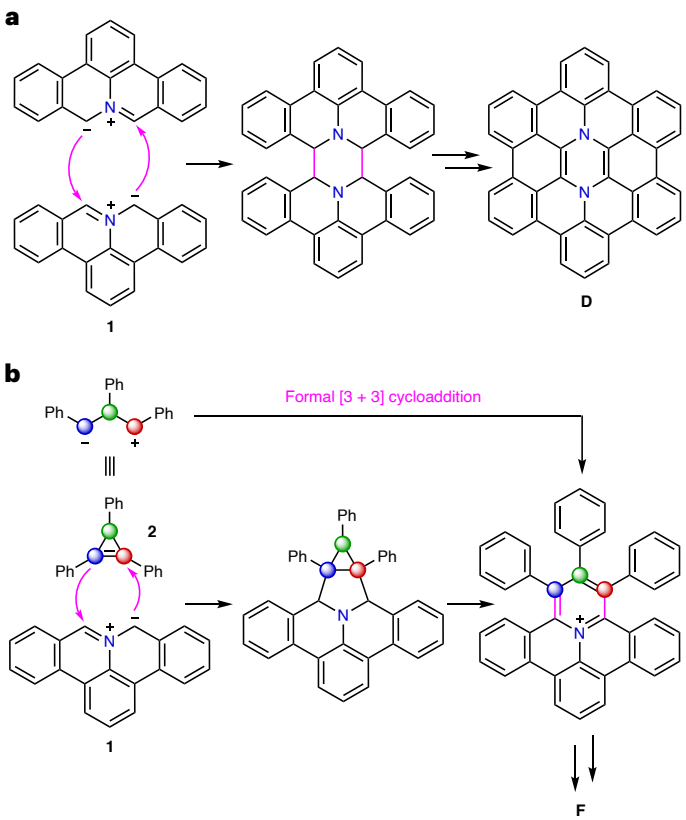

Fig. 2 | 1,3-Dipolar cycloaddition of azomethine ylides to form nitrogen-embedded HBC derivatives. a, [3 + 3] Homodimerization of azomethine ylides to form pyrazine-embedded HBC **D**[21]. **b**, Formal [3 + 3] cycloaddition of azomethine ylides and cyclopropenes as three-atomic dipolarophiles.

https://doi.org/10.1038/s44160-024-00595-5

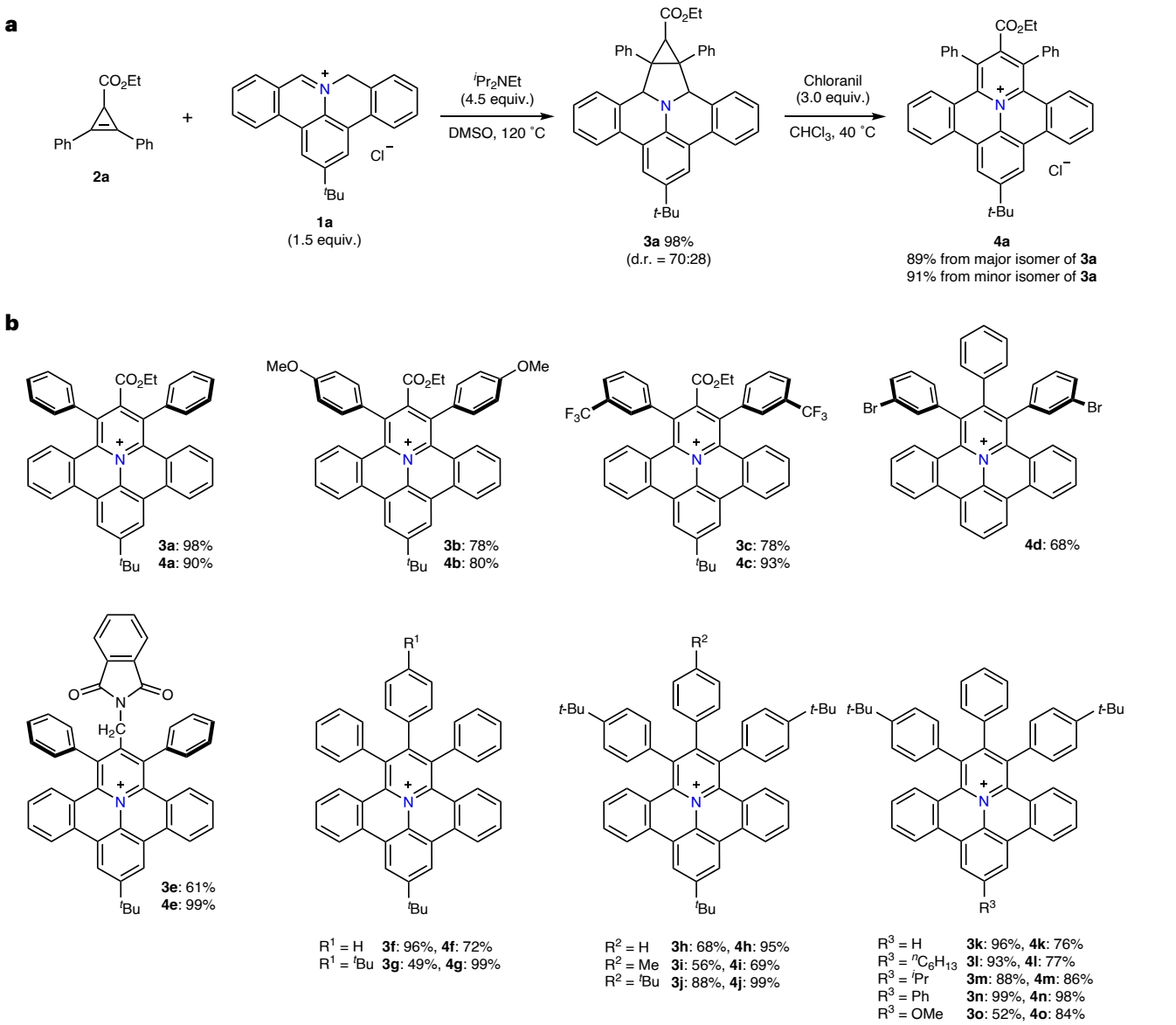

Fig. 3 | Synthesis of π-extended pyridinium derivatives. a, 1,3-Dipolar cycloaddition of azomethine ylides and cyclopropenes followed by oxidative skeletal rearrangement. **b**, Substrate scope. Counterions (Cl^-) are omitted for clarity. DMSO, dimethyl sulfoxide; d.r., diastereomeric ratio.

a wide range of substrates (Fig. 3b). Cyclopropene substrates bearing electron-donating and electron-withdrawing groups afforded **4b**–**4d** in good yields. Additionally, the phthalimide functionality was compatible under the reaction conditions to produce **4e**, indicating that alkyl substituents can also be introduced instead of alkoxycarbonyl and aryl groups. The generality of the reaction conditions was further demonstrated with various 1,2,3-triarylcyclopropene substrates, leading to the formation of triarylated π-extended pyridinium molecules **4f**–**4o** in high yields.

Synthesis and properties of azahexabenzocoronenium salts

The molecular shape of π-extended pyridinium salts **4f**–**o** prompted us to examine a dehydrogenative cyclization approach to afford azahexabenzocoronenium **5**, that is, 3a^2-azahexabenzo[*bc*,*ef*,*hi*,*kl*,*no*,*qr*]coronenium (Fig. 4). In the initial trials, Scholl reactions of **4f** using various oxidative conditions were performed, since it is a well-established strategy for promoting the cyclodehydrogenation of polycyclic aromatic molecules[36–38]. However, none of the oxidative conditions successfully afforded **5**, presumably because the electron-deficient nature of the pyridinium precursors hampered oxidation reactions (Fig. 4a, left). We then shifted our focus to cyclization under reductive conditions[39–42], which is often facilitated by mechanochemistry (Fig. 4a, right)[43]. Accordingly, the fourfold cyclodehydrogenation of **4f** was performed in the presence of excess sodium (Na) under ball milling (30 Hz) at room temperature, resulting in the formation of a black powder as a product. The matrix-assisted laser desorption/ionization (MALDI) time-of-flight mass spectrum of the crude mixture showed signals only at m/z = 580.19, which corresponds to the target molecule, azahexabenzocoronenium **5f**. However, the black powdery product did not dissolve in any solvents and could not be purified. In the next trial, therefore, we turned our attention to **4h**, which bears three *t*-butyl groups, aimed at enhancing the solubility (Fig. 4b). As anticipated, the reaction of **4h** proceeded well to produce **5h**, which shows improved solubility in organic solvents. Due to the poor crystallinity of **5h** bearing chloride as the counterion, we performed a counterion exchange reaction to obtain the corresponding borate salt, **5h′**. Likewise, we conducted mechanochemical reductive cyclization to **4k**, **4l** and **4n**, each featuring different substituents. These efforts resulted in reasonable yields of **5k**, **5l** and **5n**, respectively, expanding the scope of our synthesized compounds.

https://doi.org/10.1038/s44160-024-00595-5

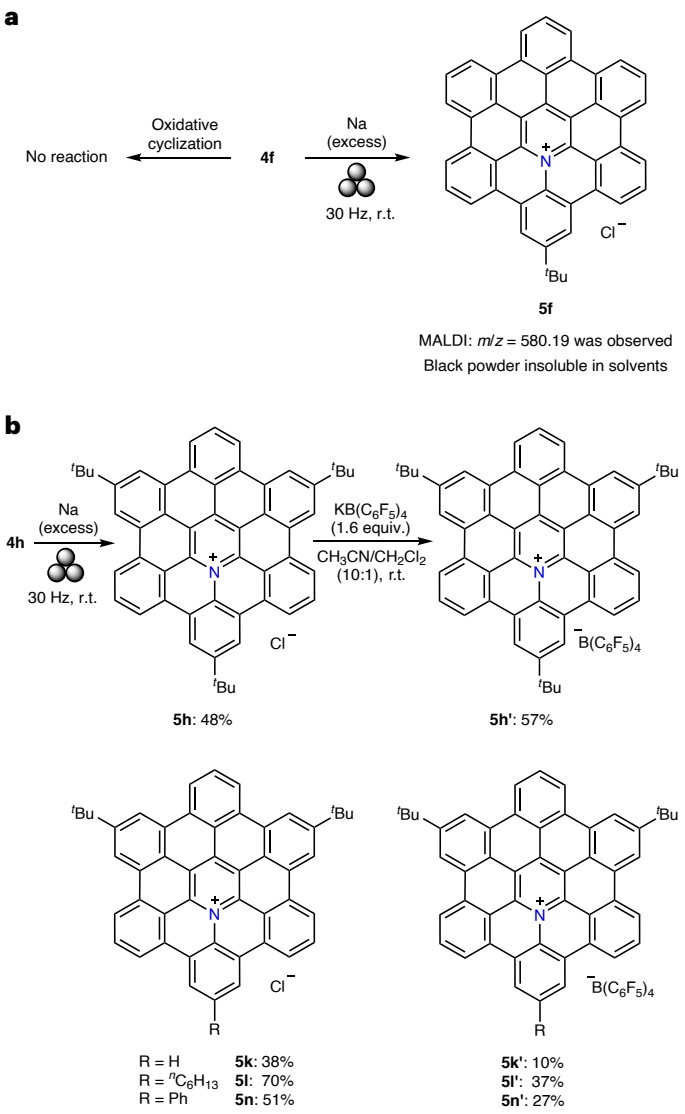

Fig. 4 | Synthesis of azahexabenzocoronenium. a, Attempted synthesis of **5f** by mechanochemical cyclization. **b**, Synthesis of **5h** and an anion exchange reaction leading to **5h′**. r.t., room temperature.

Single crystals of **5h′** were obtained by recrystallization in dichloromethane and analysed by X-ray diffraction measurement (Fig. 5). The **5h′** crystallizes in the *P* − 1 space group with four molecules and solvent molecules in the unit cell. The cationic π-core adopts a nearly planar structure with a slight wavy distortion, probably arising from the steric interaction of the *t*-butyl groups (Fig. 5a). Unfortunately, however, the crystal structure exhibits disorder in the position of the nitrogen atoms, that is, the crystal contains 1/3 of each of the three structures in Supplementary Fig. 67 as disorder. Therefore, the central pyridinium ring is observed as a regular hexagon because of averaging their structures, preventing us from discussing detailed molecular structures, including bond lengths and bond angles. Consequently, the molecular structure was determined by density functional theory (DFT) calculations at the B3LYP/6-31G(d) level of theory (Fig. 5b). The optimized structure in the gas phase has a shallow saddle shape, which would be attributed to the shorter carbon–nitrogen bonds (N–C1: 1.402 Å, N–C6: 1.429 Å) compared with the corresponding carbon–carbon bonds of HBC (1.424 and 1.448 Å, respectively) (Supplementary Fig. 68). In the crystal packing, azahexabenzocoroneniums are slip-stacked in a face-to-face manner so that each carbon atom is located near the centre of a six-membered ring in the underlying molecule (Fig. 5c). This packing arrangement closely resembles what is observed in the crystal structure of hexa-*t*-butyl-HBC[44]. The cationic cores form oblique one-dimensional columns with an interplanar distance of 3.53 Å (Fig. 5d). This value is larger than that of hexa-*t*-butyl-HBC (3.44 Å)[44] and a pyridine-fused HBC-type compound (3.36 Å)[19], which is probably attributed to the electrostatic repulsion between cationic aromatic cores. There is no interaction between the columns as the space between the columns is filled with large anions, that is, $B(C_6F_5)_4^-$ and solvent molecules.

The optical properties of compound **5h** were investigated (Fig. 6a). The absorption spectrum shows a broad absorption profile with absorption maxima at 518, 484 and 382 nm. According to time-dependent DFT calculations, the former two absorptions correspond to the HOMO/LUMO and HOMO − 1/LUMO transitions, respectively (Supplementary Fig. 74 and Supplementary Table 3) (where HOMO is the highest occupied molecular orbital and LUMO is the lowest unoccupied molecular orbital). Notably, in the case of hexabenzocoronene, the observed absorption wavelength is substantially shorter (<400 nm)[45,46]. This phenomenon can be attributed to the highly symmetrical structure of hexabenzocoronene, which results in the symmetrically forbidden nature of some low-energy transitions (referred to as α- and β-bands[47]), preventing them from contributing to longer wavelength absorption (Supplementary Fig. 73 and Supplementary Table 2). Therefore, the introduction of a nitrogen atom into the HBC core disrupts its molecular symmetry, allowing these low-energy absorptions to occur[47]. Additionally, the fluorescence of **5h** was observed in the range from 500 to 650 nm, including vibrationally resolved maxima. The fluorescence pattern mirrors the longest absorption bands. Remarkably, the Stokes shift is only 2 nm, suggesting the highly rigid structure of azahexabenzocoronenium **5h**. The fluorescence quantum yield was determined to be 30%, which is higher than that of hexabenzocoronene derivatives (typically <10%)[46]. This improvement in the emission quantum yield underscores the advantages of introducing nitrogen atoms into highly symmetric polycyclic aromatic molecules such as corannulene[48] and HBC[15,17], enhancing their fluorescence properties.

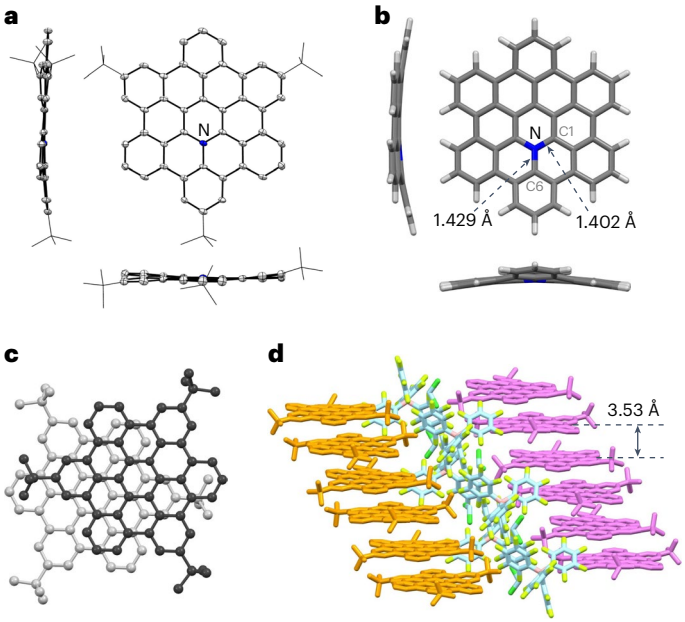

Fig. 5 | Molecular structures of azahexabenzocoronenium 5h′. a, Oak Ridge thermal-ellipsoid plot (ORTEP) structure of **5h′**. Hydrogen atoms are omitted, and *t*-butyl groups are shown as stick models for clarity. **b**, Structure of **5** determined by DFT calculation at the B3LYP/6-31G(d) level of theory. **c**, Packing structures of **5h′** with ball–stick models (top view). Only cationic moieties are shown. **d**, Packing structures of **5h′** with stick models (side view).

https://doi.org/10.1038/s44160-024-00595-5

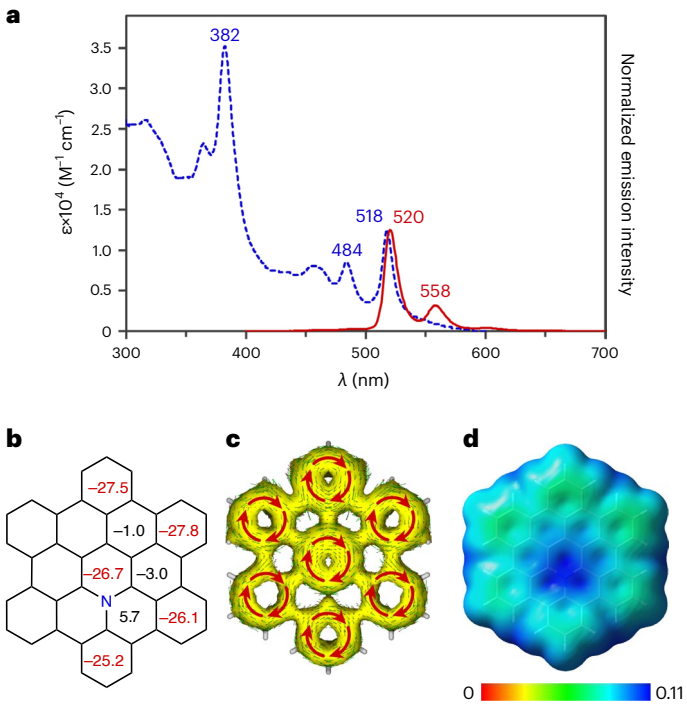

Fig. 6 | Molecular properties of azahexabenzocoronenium 5. a, Ultraviolet–visible absorption (dotted blue line) and normalized emission (solid red line; excitation wavelength 350 nm) spectra of azahexabenzocoronenium **5h** (5.6×10^{-6} M) in dichloromethane. **b**, $NICS(1)_{zz}$ values of **5** calculated at the B3LYP/6-31G(d) level of theory. Values were determined by averaging those on the back and front of the curved surface of **5**. **c**, ACID plot of **5** calculated at the B3LYP/6-31G(d) level of theory with an isovalue of 0.005. The observed ring currents are shown with curved red arrows. **d**, Electrostatic potential (ESP) map of **5** calculated at the B3LYP/6-31G(d) level of theory, which indicates the electron density on the molecular surface.

The aromaticity and electronic properties of **5** were investigated by DFT calculations. Nucleus-independent chemical shift (NICS) analysis revealed a value of −26.7 at the central pyridinium ring, with values ranging from −25.2 to −27.5 at the peripheral benzene rings, which indicates that they are aromatic (Fig. 6b). Indeed, the anisotropy of the induced current density (ACID) plot shows the presence of 6π clockwise ring currents along the central pyridinium and peripheral six benzene rings (Fig. 6c). These findings provide compelling evidence that the aromatic nature of **5** closely resembles that of the parent HBC (Supplementary Figs. 71 and 72). Additionally, electrostatic map analysis indicated that the cationic charge is localized around the internal nitrogen atom (Fig. 6d).

Synthesis of azahexabenzocoronenium-based graphene nanoribbons

To expand the application of azahexabenzocoronenium **5**, we decided to perform its oligomerization on metal surfaces to fabricate chevron-like nitrogen-containing graphene nanoribbons (GNRs; Fig. 7a). Several examples of HBC-based chevron-like GNRs bearing nitrogen atoms in their periphery have been reported in the literature[49–55], but there are fewer examples of HBC-based chevron-like GNRs bearing internal nitrogen atoms[56]. Initially, precursor **4d** was sublimed in situ onto a clean Au(111) surface under ultrahigh vacuum conditions. The large-scale scanning tunnelling microscopy (STM) topography (Fig. 7b) shows that the cationic part of **4d** assembles into distinct small clusters, while no chlorine atoms were detected on the metal surface (Supplementary Fig. 77)[22]. A high-resolution STM topography of one of these clusters is shown in the inset of Fig. 7b. Subsequently, the sample underwent annealing at 150 °C, inducing an intermolecular Ullmann-type cross-coupling reaction to form the polymer intermediate (Fig. 7c). The high-resolution image of the polymer (Fig. 7c, inset) reveals a periodicity of 0.88 nm, indicating the formation of covalent bonds between the precursor molecules. The bright spots observed in the middle of the polymer chain arise from the steric effect of the out-of-plane phenyl rings. Further elevating the annealing temperature to 400 °C resulted in complete planarization of the linear structures (Fig. 7d). High-resolution STM topographies (Fig. 7e–g) of these products with varying lengths demonstrate the successful synthesis of the desired oligomers depicted in Fig. 7a, although some oligomers with defects were also observed (Supplementary Fig. 75). Bond-resolved STM imaging with a CO-functionalized tip (Fig. 7h–j) clearly confirmed the formation of the desired GNRs, providing direct and compelling evidence that the synthetic concept illustrated in Fig. 7a was successfully realized. It is noteworthy that the selective introduction of nitrogen atoms is ensured by a darker contrast around the nitrogen atoms, which was reported in previous studies[22,57,58]. In addition, the electronic properties of the GNRs were measured by scanning tunnelling spectroscopy with a metal tip, which revealed that their band gap gradually decreased with increasing number of aza-HBC units (Supplementary Fig. 76). To further clarify the electronic structure and charge state of GNRs, we performed a series of theoretical calculations of GNRs with increasing numbers of positive charges using the vacuum level to align the Fermi energy between them and the ideal Au (111) surface. Supplementary Fig. 79a, 79b and 79c shows the density of states of the GNRs in the gas phase with charges of 0, +1 and +2 per 2N site unit cell, respectively. As shown in Supplementary Fig. 81a, the d*I*/d*V* spectrum of the GNRs on the gold surface was also calculated and found to be in the best agreement for the gas-phase system with +1 charges. This is further confirmed by calculating the charge transfer between the GNR and the gold surface (Supplementary Fig. 81b), where a decrease in positive charge at the nitrogen sites and an associated accumulation of positive charge at the gold site directly below it are observed. The simulated contrasts in Supplementary Figs. 80 and 81c are in reasonable agreement with those shown in Supplementary Fig. 76. These results led to the conclusion that the local positive charge on each azahexabenzocoronenium unit of the GNRs is +0.5. It was reported that a dicationic diaza-HBC molecule adopts a dicationic state on the Au(111) surface[22] and that neutral nitrogen-embedded PAH molecules adsorbed on the Au(111) surface are positively charged due to the charge transfer from the neutral molecules to the underlying metal substrate[56,57]. Given these reports, it is reasonable to conclude that the present GNRs have +0.5 charge per aza-HBC unit.

Conclusions

In summary, we have developed a synthetic approach for accessing heteroatom-embedded HBC derivatives. The key to the successful synthesis of 3a[2]-azahexa-*peri*-hexabenzocoronenium lies in the formal [3 + 3] cycloaddition of polycyclic azomethine ylides with cyclopropene derivatives, followed by mechanochemical intramolecular cyclization. A comprehensive investigation of the optical and electronic properties of the resulting molecules was performed through spectroscopic analyses as well as theoretical calculations. Furthermore, we extended our methodology to synthesize chevron-like 3a[2]-azahexa-*peri*-hexabenzocoronenium GNRs through on-surface synthesis and elucidated their electronic structure and charge state experimentally and theoretically. The present versatile approach opens possibilities for the utilization of heteroatom-embedded hexabenzocoronene derivatives in various potential applications.

Methods

1,3-Dipolar cycloaddition of azomethine ylides 1 and cyclopropenes 2

To a pre-heated solution of cyclopropene **2** (0.10 mmol) and iminium salt **1** (0.15 mmol) in dimethyl sulfoxide (3.0 ml) at 120 °C was added

https://doi.org/10.1038/s44160-024-00595-5

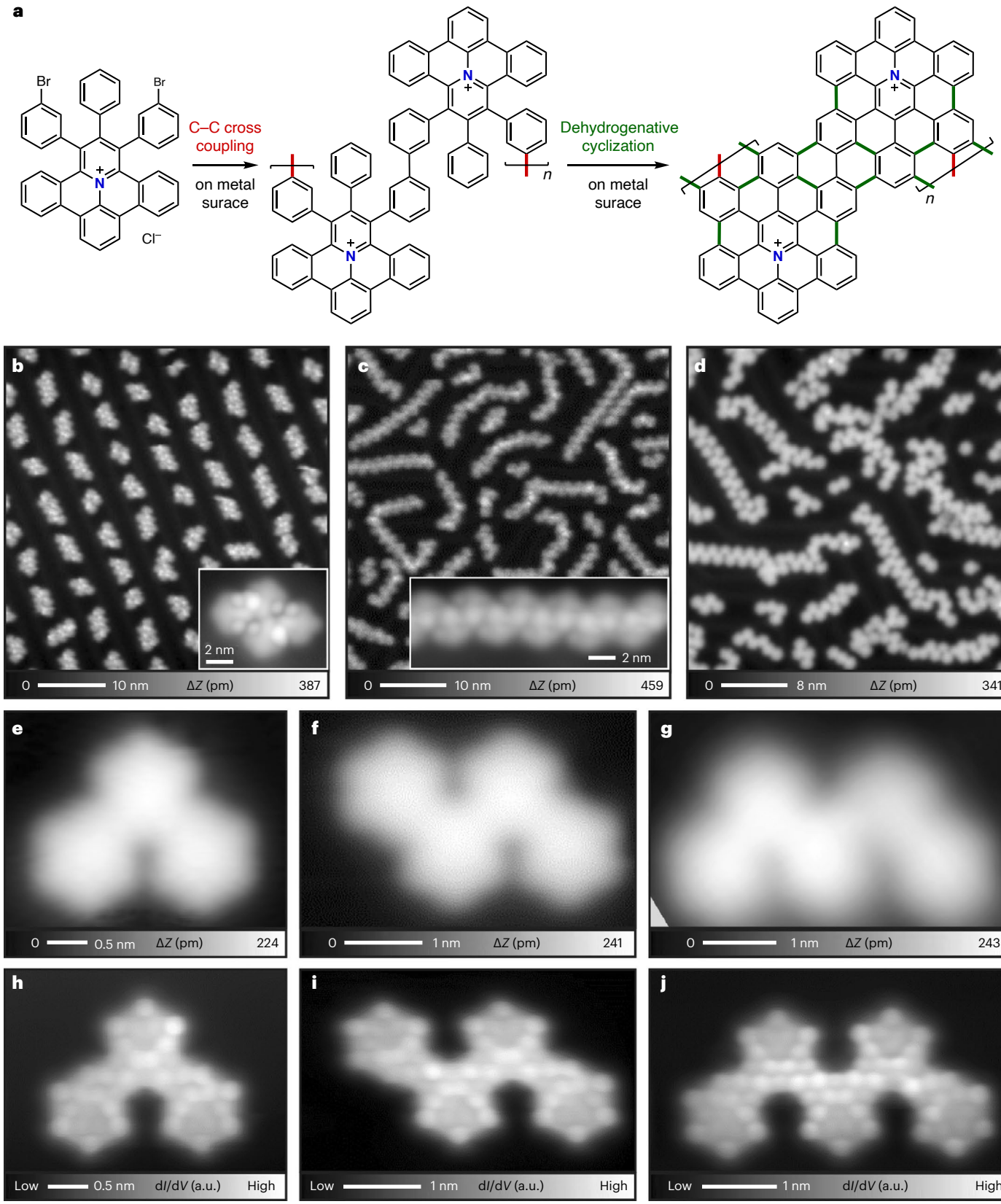

Fig. 7 | On-surface synthesis of azahexabenzocoronenium-based GNRs. **a**, On-surface oligomerization of azahexabenzocoronenium precursor **4d** via Ullmann-type coupling and cyclodehydrogenation. **b**, Overview STM topography of as-deposited **4d** on Au(111). Inset, high-resolution STM image of the self-assembled clusters. **c**, Overview STM topography after annealing at 150 °C. Inset, high-resolution STM image of the polymer. **d**, Overview STM topography after annealing at 400 °C. **e**, High-resolution STM topography of GNR trimer. **f**, High-resolution STM topography of GNR tetramer. **g**, High-resolution STM topography of GNR pentamer. **h**, Bond-resolved STM image of GNR trimer. **i**, Bond-resolved STM image of GNR tetramer. **j**, Bond-resolved STM image of GNR pentamer. Measurement parameters: $V = 200$ mV and $I = 10$ pA (**b**–**g**), and $V = 0$ mV (**h**–**j**).

N,*N*-diisopropyl(ethyl)amine (0.45 mmol). The mixture was stirred for 14 h at 120 °C, cooled to room temperature and poured into toluene (30 ml). The organic phase was washed with brine (10 ml, 3×), dried over sodium sulfate and concentrated under reduced pressure. The crude mixture was purified by silica gel chromatography to obtain cycloadduct **3** as a mixture of diastereomers.

Oxidative aromatization of 3 to synthesize π-extended pyridinium 4

To a solution of compound **3** (0.050 mmol, a mixture of stereoisomers) in chloroform (3.0 ml) was added chloranil (0.15 mmol) at room temperature. The mixture was stirred for 3 h at 40 °C and cooled to room temperature. After being concentrated under reduced pressure, the crude mixture was purified by silica-gel chromatography (methanol/dichloromethane) to obtain π-extended pyridinium **4**.

Mechanochemical cyclization of 4 to synthesize azahexabenzocoronenium 5

To a 15 ml stainless-steel jar was added **4** (10 mg, 13–14 µmol), sodium (10 mg, 0.4 mmol) and a stainless-steel ball. The jar was closed and milled at 30 Hz for 30 min. The reaction mixture was collected with chloroform, and the organic layers were concentrated under reduced pressure. The crude mixture was purified by silica-gel column chromatography (methanol/dichloromethane) to obtain azahexabenzocoronenium **5**.

Data availability

The data supporting the findings of the current study are available within the paper and its Supplementary Information. The crystallographic data for structures reported in this study for compounds **3a**, **4a** and **5h′** have been deposited at the Cambridge Crystallographic Data Centre (CCDC), under accession numbers 2293773 (for **3a**), 2293774 (for **4a**) and 2293775 (for **5h′**). These data can be obtained free of charge from The Cambridge Crystallographic Data Centre via www.ccdc.cam.ac.uk/data_request/cif.

References

1. Clar, E. & Ironside, C. T. Hexabenzocoronene. *Proc. Chem. Soc.* https://doi.org/10.1039/PS9580000329 (1958).
2. Clar, E., Ironside, C. T. & Zander, M. The electronic interaction between benzenoid rings in condensed aromatic hydrocarbons. 1:12-2:3-4:5-6:7-8:9-10:11-hexabenzocoronene, 1:2-3:4-5:6-10:11-tetrabenzoanthanthrene, and 4:5-6:7-11:12-13:14-tetrabenzoperopyrene. *J. Chem. Soc.* https://doi.org/10.1039/JR9590000142 (1959).
3. Wu, J., Pisula, W. & Müllen, K. Graphenes as potential material for electronics. *Chem. Rev.* **107**, 718–747 (2007).
4. Seyler, H., Purushothaman, B., Jones, D. J., Holmes, A. B. & Wong, W. W. H. Hexa-*peri*-hexabenzocoronene in organic electronics. *Pure Appl. Chem.* **84**, 1047–1067 (2012).
5. Kumar, S. & Tao, Y.-T. Coronenes, benzocoronenes and beyond: modern aspects of their syntheses, properties, and applications. *Chem. Asian J.* **16**, 621–647 (2021).
6. Hill, J. P. et al. Self-assembled hexa-*peri*-hexabenzocoronene graphitic nanotube. *Science* **304**, 1481–1483 (2004).
7. Ishiwari, F., Shoji, Y. & Fukushima, T. Supramolecular scaffolds enabling the controlled assembly of functional molecular units. *Chem. Sci.* **9**, 2028–2041 (2018).
8. Lin, F.-J., Chen, H.-H. & Tao, Y.-T. Molecularly aligned hexa-*peri*-hexabenzocoronene films by brush-coating and their application in thin-film transistors. *ACS Appl. Mater. Interfaces* **11**, 10801–10809 (2019).
9. Lin, F.-J., Yang, C.-W., Chen, H.-H. & Tao, Y.-T. Alignment and photopolymerization of hexa-*peri*-hexabenzocoronene derivatives carrying diacetylenic side chains for charge-transporting application. *J. Am. Chem. Soc.* **142**, 11763–11771 (2020).
10. Yin, M. et al. Functionalization of self-assembled hexa-*peri*-hexabenzocoronene fibers with peptides for bioprobing. *J. Am. Chem. Soc.* **131**, 14618–14619 (2009).
11. Zilberman, Y. et al. Carbon nanotube/hexa-*peri*-hexabenzocoronene bilayers for discrimination between nonpolar volatile organic compounds of cancer and humid atmospheres. *Adv. Mater.* **22**, 4317–4320 (2010).
12. Stępień, M., Gońka, E., Żyła, M. & Sprutta, N. Heterocyclic nanographenes and other polycyclic heteroaromatic compounds: synthetic routes, properties, and applications. *Chem. Rev.* **117**, 3479–3716 (2017).
13. Wang, X.-Y., Yao, X., Narita, A. & Müllen, K. Heteroatom-doped nanographenes with structural precision. *Acc. Chem. Res.* **52**, 2491–2505 (2019).
14. Borissov, A. et al. Recent advances in heterocyclic nanographenes and other polycyclic heteroaromatic compounds. *Chem. Rev.* **122**, 565–788 (2022).
15. Draper, S. M., Gregg, D. J. & Madathil, R. Heterosuperbenzenes: a new family of nitrogen-functionalized, graphitic molecules. *J. Am. Chem. Soc.* **124**, 3486–3487 (2002).
16. Draper, S. M. et al. Complexed nitrogen heterosuperbenzene: the coordinating properties of a remarkable ligand. *J. Am. Chem. Soc.* **126**, 8694–8701 (2004).
17. Wijesinghe, L. P. et al. [2+2+2] Cyclotrimerisation as a convenient route to 6N-doped nanographenes: a synthetic introduction to hexaazasuperbenzenes. *RSC Adv.* **7**, 24163–24167 (2017).
18. Graczyk, A. et al. Terpyridine-fused polyaromatic hydrocarbons generated via cyclodehydrogenation and used as ligands in Ru(II) complexes. *Dalton Trans.* **41**, 7746–7754 (2012).
19. Reger, D., Schöll, K., Hampel, F., Maid, H. & Jux, N. Pyridinic nanographenes by novel precursor design. *Chem. Eur. J.* **27**, 1984–1989 (2021).
20. Krieg, M. et al. Construction of an internally B_3N_3-doped nanographene molecule. *Angew. Chem. Int. Ed.* **54**, 8284–8286 (2015).
21. Wang, X.-Y. et al. Exploration of pyrazine-embedded antiaromatic polycyclic hydrocarbons generated by solution and on-surface azomethine ylide homocoupling. *Nat. Commun.* **8**, 1948 (2017).
22. Biswas, K. et al. On-surface synthesis of a dicationic diazahexabenzocoronene derivative on the Au(111) surface. *Angew. Chem. Int. Ed.* **60**, 25551–25556 (2021).
23. Dosso, J. et al. Synthesis and optoelectronic properties of hexa-*peri*-hexabenzoborazinocoronene. *Angew. Chem. Int. Ed.* **56**, 4483–4487 (2017).
24. Dosso, J. et al. Boron–nitrogen-doped nanographenes: a synthetic tale from borazine precursors. *Chem. Eur. J.* **26**, 6608–6621 (2019).
25. Berger, R. et al. Synthesis of nitrogen-doped zigzag-edge peripheries: dibenzo-9*a*-azaphenalene as repeating unit. *Angew. Chem. Int. Ed.* **53**, 10520–10524 (2014).
26. Ito, S., Tokimaru, Y. & Nozaki, K. Isoquinolino[4,3,2-*de*] phenanthridine: synthesis and its use in 1,3-dipolar cycloadditions to form nitrogen-containing polyaromatic hydrocarbons. *Chem. Commun.* **51**, 221–224 (2015).
27. Berger, R., Wagner, M., Feng, X. & Müllen, K. Polycyclic aromatic azomethine ylides: a unique entry to extended polycyclic heteroaromatics. *Chem. Sci.* **6**, 436–441 (2015).
28. Tokimaru, Y., Ito, S. & Nozaki, K. Synthesis of pyrrole-fused corannulenes: 1,3-dipolar cycloaddition of azomethine ylides to corannulene. *Angew. Chem. Int. Ed.* **56**, 15560–15564 (2017).
29. Dumele, O. et al. Photocatalytic aqueous CO_2 reduction to CO and CH_4 sensitized by ullazine supramolecular polymers. *J. Am. Chem. Soc.* **144**, 3127–3136 (2022).
30. Zhang, X., Mackinnon, M. R., Bodwell, G. J. & Ito, S. Synthesis of a π-extended azacorannulenophane enabled by strain-Induced 1,3-dipolar cycloaddition. *Angew. Chem. Int. Ed.* **61**, e202116585 (2022).

31. Li, S. et al. 1,3-Dipolar cycloaddition of polycyclic azomethine ylide to norcorroles: towards dibenzoullazine-fused derivatives. *Chem. Commun.* **58**, 6510–6513 (2022).
32. Hager, J. et al. Acenaphthylene-fused ullazines: fluorescent π-extended monopyrroles with tunable electronic gaps. *Org. Chem. Front.* **9**, 3179–3185 (2022).
33. Ikeda, H., Hoshi, Y. & Miyashi, T. 1,3-Bis(4-methoxyphenyl) cyclohexane-1,3-diyl cation radical: divergent reactivity depending upon electron-transfer conditions. *Tetrahedron Lett.* **42**, 8485–8488 (2001).
34. Gaucher, X., Jida, M. & Ollivier, J. Concise total asymmetric synthesis of (*S*)-2-phenylpiperidin-3-one. *Synlett* **20**, 3320–3322 (2009).
35. Xu, W.-B., Li, C. & Wang, J. Rh^{I}-catalyzed carbonylative [3+1] construction of cyclobutenones via C–C σ-bond activation of cyclopropenes. *Chem. Eur. J.* **24**, 15786–15790 (2018).
36. Grzybowski, M., Skonieczny, K., Butenschön, H. & Gryko, D. T. Comparison of oxidative aromatic coupling and the Scholl reaction. *Angew. Chem. Int. Ed.* **52**, 9900–9930 (2013).
37. Grzybowski, M., Sadowski, B., Butenschön, H. & Gryko, D. T. Synthetic applications of oxidative aromatic coupling—from biphenols to nanographenes. *Angew. Chem. Int. Ed.* **59**, 2998–3027 (2020).
38. Jassas, R. S. et al. Scholl reaction as a powerful tool for the synthesis of nanographenes: a systematic review. *RSC Adv.* **11**, 32158–32202 (2021).
39. Schlichting, P., Rohr, U. & Müllen, K. Easy synthesis of liquid crystalline perylene derivatives. *J. Mater. Chem.* **8**, 2651–2655 (1998).
40. Gryko, D. T., Piechowska, J. & Gałęzowski, M. Strongly emitting fluorophores based on 1-azaperylene scaffold. *J. Org. Chem.* **75**, 1297–1300 (2010).
41. Rickhaus, M., Belanger, A. P., Wegner, H. A. & Scott, L. T. An oxidation induced by potassium metal. Studies on the anionic cyclodehydrogenation of 1,1′-binaphthyl to perylene. *J. Org. Chem.* **75**, 7358–7364 (2010).
42. Kawahara, K. P., Matsuoka, W., Ito, H. & Itami, K. Synthesis of nitrogen-containing polyaromatics by aza-annulative π-extension of unfunctionalized aromatics. *Angew. Chem. Int. Ed.* **59**, 6383–6388 (2020).
43. Wang, C.-S., Sun, Q., García, F., Wang, C. & Yoshikai, N. Robust cobalt catalyst for nitrile/alkyne [2+2+2] cycloaddition: synthesis of polyarylpyridines and their mechanochemical cyclodehydrogenation to nitrogen-containing polyaromatics. *Angew. Chem. Int. Ed.* **60**, 9627–9634 (2021).
44. Herwig, P. T., Enkelmann, V., Schmelz, O. & Müllen, K. Synthesis and structural characterization of hexa-*tert*-butyl-hexa-*peri*-hexabenzocoronene, its radical cation salt and its tricarbonylchromium complex. *Chem. Eur. J.* **6**, 1834–1839 (2020).
45. Nagase, M., Kato, K., Yagi, Y., Segawa, Y. & Itami, K. Six-fold C–H borylation of hexa-*peri*-hexabenzocoronene. *Beilstein J. Org. Chem.* **16**, 391–397 (2020).
46. Hu, Y. et al. Spiro-fused bis-hexa-*peri*-hexabenzocoronene. *Chem. Commun.* **54**, 13575–13578 (2018).
47. Kastler, M., Schmidt, J., Pisula, W., Sebastiani, D. & Müllen, K. From armchair to zigzag peripheries in nanographenes. *J. Am. Chem. Soc.* **128**, 9526–9534 (2006).
48. Ito, S., Tokimaru, Y. & Nozaki, K. Benzene-fused azacorannulene bearing an internal nitrogen atom. *Angew. Chem. Int. Ed.* **54**, 7256–7260 (2015).
49. Bronner, C. et al. Aligning the band gap of graphene nanoribbons by monomer doping. *Angew. Chem. Int. Ed.* **52**, 4422–4425 (2013).
50. Vo, T. H. et al. Bottom-up solution synthesis of narrow nitrogen-doped graphene nanoribbons. *Chem. Commun.* **50**, 4172–4174 (2014).
51. Zhang, Y. et al. Direct visualization of atomically precise nitrogen-doped graphene nanoribbons. *Appl. Phys. Lett.* **105**, 023101 (2014).
52. Cai, J. et al. Graphene nanoribbon heterojunctions. *Nat. Nanotechnol.* **9**, 896–900 (2014).
53. Vo, T. H. et al. Nitrogen-doping induced self-assembly of graphene nanoribbon-based two-dimensional and three-dimensional metamaterials. *Nano Lett.* **15**, 5770–5777 (2015).
54. Marangoni, T., Haberer, D., Rizzo, D. J., Cloke, R. R. & Fischer, F. R. Heterostructures through divergent edge reconstruction in nitrogen-doped segmented graphene nanoribbons. *Chem. Eur. J.* **22**, 13037–13040 (2016).
55. Durr, R. A. et al. Orbitally matched edge-doping in graphene nanoribbons. *J. Am. Chem. Soc.* **140**, 807–813 (2018).
56. Wen, E. C. H. et al. Magnetic interactions in substitutional core-doped graphene nanoribbons. *J. Am. Chem. Soc.* **144**, 13696–13703 (2022).
57. Wang, T. et al. Aza-triangulene: on-surface synthesis and electronic and magnetic properties. *J. Am. Chem. Soc.* **144**, 4522–4529 (2022).
58. Lawrence, J. et al. Topological design and synthesis of high-spin aza-triangulenes without Jahn–Teller distortions. *ACS Nano* **17**, 20237–20245 (2023).

Acknowledgements

This work was supported by Nanyang Technological University (NTU), the Ministry of Education, Singapore, under its Academic Research Fund Tier 1 (RG2/23) for S.I. and the Japan Society for the Promotion of Science (JSPS) KAKENHI grant number 22H00285 for S.K. Computing resources from the NTU High Performance Computing Team are gratefully acknowledged. We thank Y. Li (NTU) for his support with the X-ray diffraction analysis and O. J. Silveira (Aalto University) for valuable discussion on the theoretical calculations.

Author contributions

S.I. directed and conceived the project and performed the theoretical studies with DFT calculations. X.Z., C.C.H.T., F.H. and Y.H. performed all the experimental work and data collection in organic synthesis. D.L. and S.K. performed the STM experiments and analysed the results. A.S.F. performed theoretical calculations of the GNRs deposited on the metal surface. All the authors discussed the results and contributed to the preparation of the manuscript.

Competing interests

The authors declare no competing interests.

Additional information

Supplementary information The online version contains supplementary material available at https://doi.org/10.1038/s44160-024-00595-5.

Correspondence and requests for materials should be addressed to Adam S. Foster, Shigeki Kawai or Shingo Ito.

Peer review information *Nature Synthesis* thanks the anonymous reviewers for their contribution to the peer review of this work. Primary Handling Editor: Thomas West, in collaboration with the *Nature Synthesis* team.